ELSEVIER

Journal of Nuclear Materials 307–311 (2002) 266–271

journal of nuclear materials

www.elsevier.com/locate/jnucmat

Microstructural evolution in modified 9Cr–1Mo ferritic/martensitic steel irradiated with mixed high-energy proton and neutron spectra at low temperatures

B.H. Sencer [a,*], F.A. Garner [b], D.S. Gelles [b], G.M. Bond [c], S.A. Maloy [d]

[a] *Nuclear Engineering and Radiological Science, University of Michigan, 1906 Cooley Building 2355 Bonisteel Boulevard, Ann Arbor, MI 48108-2104, USA*

[b] *Pacific Northwest National Laboratory, Richland, WA 99352, USA*

[c] *New Mexico Institute of Mining and Technology, Socorro, NM 87801, USA*

[d] *Los Alamos National Laboratory, Los Alamos, NM 87545, USA*

Abstract

Modified 9Cr–1Mo ferritic/martensitic steel was exposed at 32–57 °C to a mixed proton/neutron particle flux and spectrum at the Los Alamos Neutron Science Center. The microstructure of unirradiated 9Cr–1Mo consists of laths, dislocations and carbides. Examination of electron diffraction patterns obtained from extraction replicas of unirradiated 9Cr–1Mo revealed that the precipitate microstructure was primarily dominated by $M_{23}C_6$ carbides. The post-irradiation microstructure contained black-spot damage in addition to precipitates and dislocations. Examination of electron diffraction patterns revealed diffuse rings from $M_{23}C_6$ carbides, indicating amorphization and/or nanocrystallinity. Crystalline MC carbides were also found. No cavity formation was found although a significant amount of helium and hydrogen generation had been generated. TEM–EDS examination of extraction replicas for carbides from unirradiated and irradiated samples did not show any detectable changes in composition of either $M_{23}C_6$ or MC carbides. There was also no evident change in carbide size. Lattice images of $M_{23}C_6$ carbides revealed an amorphous microstructure following irradiation, but MC carbides were still crystalline.

1. Introduction

Ferritic and ferritic/martensitic steels may play a significant role as structural components for various proposed fusion and accelerator-driven fusion hybrid reactors operating at high temperatures and high neutron-induced damage rates. However, most of the data on irradiated material for this class of steels were derived only with neutron irradiation at relatively high temperatures and doses characteristic of first wall applications. Accelerator-driven hybrids and various spallation neutron devices will also use ferritic/martensitic steels in some regions operating at much lower temperatures. An example of such an application is the beam window for entry of the high-energy protons into the reactor system. Research on structural materials operating at lower temperatures has been conducted by the accelerator production of tritium (APT) project [1].

In the APT, target and blanket components will be exposed to the primary proton beam with an energy of ~1.2 GeV, while other parts of the target/blanket assembly will be exposed primarily to protons, to a mixed proton-neutron flux, or only to neutrons. The APT target assembly is designed to operate at relatively low temperatures ($\leqslant 150$ °C) and pressures. Only a limited database on effects of proton irradiation on material properties is available for applications in this environment. To investigate the effects of these conditions on the microstructurural evolution, TEM discs of 9Cr–1Mo

* Corresponding author. Tel.: +1-734 764 5290; fax: +1-734 763 4540.

E-mail address: sencer@umich.edu (B.H. Sencer).

0022-3115/02/$ - see front matter © 2002 Published by Elsevier Science B.V.
PII: S0022-3115(02)01198-4

were exposed to a particle flux and spectrum at the Los Alamos Neutron Science Center (LANSCE) that closely match those expected in APT.

This paper describes the microstructure and especially phase stability of $M_{23}C_6$ and MC carbides in modified 9Cr–1Mo ferritic/martensitic steel at 0.5–9.6 dpa and temperatures of 32–57 °C.

2. Experimental procedure

The alloy 9Cr–1Mo is a ferritic/martensitic alloy with a nominal composition of 0.002%Al, 0.089%C, 9.24%Cr, 0.08%Cu, Bal. Fe, 0.47%Mn, 0.96%Mo, 0.16%Ni, 0.021%P, 0.006%S, 0.28%Si, 0.002%Ti, 0.21%V, 0.054%Nb, 0.019%Co, 0.01%W, 0.035%N, 0.008%O, in weight percent. Specimens examined in this study were prepared by electrodischarge-machining standard 3 mm diameter 0.25 μm thick transmission electronic microscope TEM disks. These specimens were normalized at 1038 °C for 1 h and air-cooled, and then tempered at 760 °C for 1 h and air-cooled to room temperature.

The irradiation was conducted in the LANSCE facility at Los Alamos National Laboratory. Details of the irradiation were published previously [1]. In this irradiation series there was a Gaussian proton beam having a circular intensity profile of $2\sigma = 3$ cm over the specimen ensemble. There were also high-energy spallation neutrons existing at lower flux [2]. Doses were determined through analysis of the isotopes produced in activation foils placed alongside the specimens. The irradiation temperatures were determined from thermocouples placed in each irradiation tube [3]. Three irradiated specimens at different exposure levels were chosen for evaluation. The irradiation temperature varied somewhat with dose rate, such that the temperature was 32 °C at the lowest dose (0.5 dpa), 46 °C at 1.1 dpa and 57 °C at 9.6 dpa.

Thin foil samples were prepared for TEM examination by conventional jet electropolishing methods, in 5% perchloric acid, 95% methanol, at −20 °C and 50 V. TEM examinations were conducted with a JEOL 1200EX (120 keV) for microstructural characterization and energy-dispersive X-ray spectrometry (EDS), and a JEOL 2010F (FEG-STEM, 200 keV) for high resolution.

3. Results

3.1. Microstructural evolution

The microstructure of unirradiated 9Cr–1Mo contains a duplex structure of martensite and ferrite prior to irradiation, as shown in Fig. 1(a), a prior austenitic boundary was also decorated with carbides. Fig. 1(b) shows the dislocation structure in the martensitic laths in bright-field contrast. Carbides distributed at and around subgrain boundaries are shown in bright-field (Fig. 2(a)) and dark-field contrast (Fig. 2(b)). All the carbides have the same orientation relationship with the matrix. Electron diffraction patterns obtained from extraction replicas revealed that $M_{23}C_6$ dominated the precipitate microstructure of the alloy. Resent study of matrix carbides in F82H ferritic/martensitic steel showed coherent interface between carbide and the matrix [4].

The irradiation resulted in the formation of black-spot damage, which was present in all specimens. Fig. 2(c) shows black-spot damage and dislocation structure in dark-field contrast at 1.1 dpa. Subgrain boundaries remained unchanged, as shown in Fig. 2(d). Radiation-induced precipitation did not occur. The possibility of cavity formation was investigated in Fresnel contrast. This technique enables the detection of cavities as small as 1 nm [5]. However, no cavity (bubble and/or void) formation was found in the specimens examined between 0.5 and 9.6 dpa.

$M_{23}C_6$ carbides were found to lose their crystalline stability with high-energy irradiation. The $M_{23}C_6$

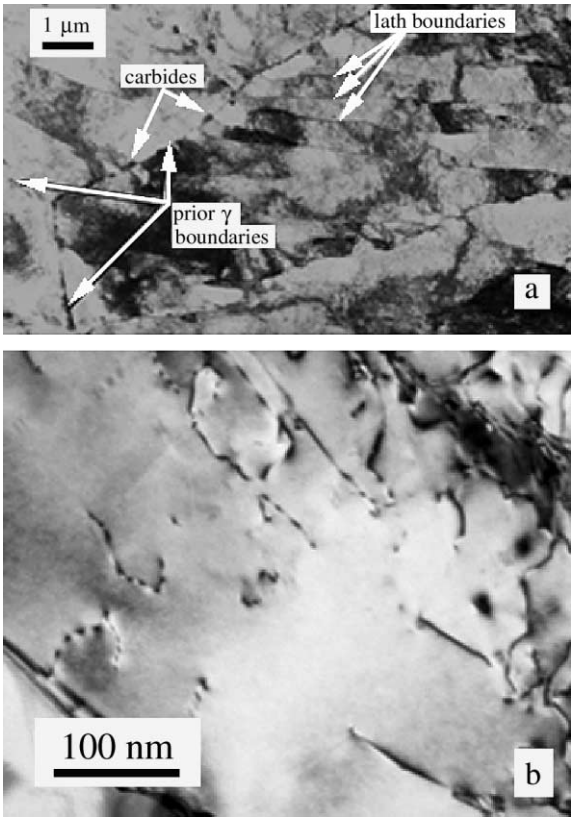

Fig. 1. Microstructure of 9Cr–1Mo alloy prior to proton irradiation. (a) The martensite reaction has taken place and carbides have formed during tempering. (b) Bright-field contrast showing dislocation structure in the martensitic laths $g = 200$.

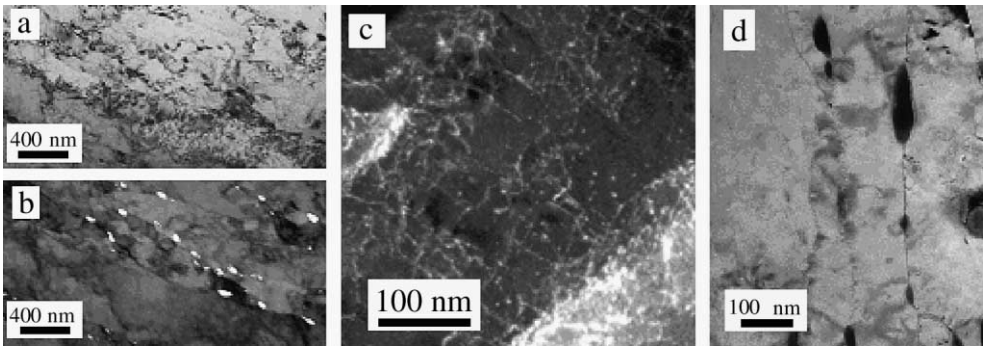

Fig. 2. Carbide distribution around subgrains in unirradiated 9Cr–1Mo, (a) in bright-field contrast and (b) in precipitate dark-field contrast. TEM images of (a) and (b) are from the same region. All these carbides have the same orientation relationship. (c) Dark-field contrast ($g = 200$) in irradiated 9Cr–1Mo, the black-spot damage and dislocations at 1.1 dpa. (d) Bright-field contrast showing martensitic laths at 1.1 dpa.

carbides produced diffuse diffraction rings at doses as low as 0.5 dpa, suggesting that the precipitates are amorphous and/or nanocrystalline as shown in Fig. 3. Fig. 3(a) and (b) show bright-field and dark-field images of $M_{23}C_6$ carbides. Fig. 3(b) is imaged with the diffuse ring marked with arrow 1 in Fig. 3(d). However MC carbides were still crystalline after irradiation, as shown in Fig. 3(c) in bright-field, and from the extra spot from MC carbide in diffraction pattern indicated with arrow 2 in Fig. 3(d). MC carbides remained crystalline at increasing dose, as shown in Fig. 3 for 1.1 dpa. Fig. 3(e), (f), and (g) show a bright-field image, the corresponding electron diffraction pattern, and a precipitate dark-field image of Nb-rich MC carbides respectively. MC carbide size (an average size of ~50 nm) was unchanged by irradiation. This is in agreement with literature [4]. The $M_{23}C_6$ carbide size (an average size of ~100 nm) also appeared to be unchanged after irradiation as shown in

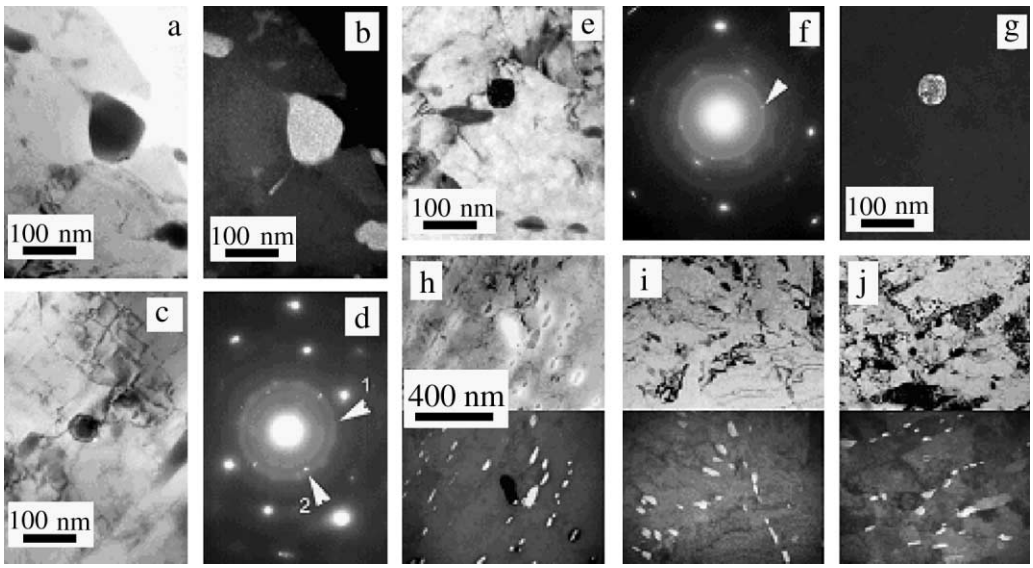

Fig. 3. $M_{23}C_6$ carbides show diffuse diffraction rings at 0.5 dpa. The carbides are imaged (a) in bright-field and (b) in dark-field contrast from the outer ring in (d) (arrow 1). An MC carbide can also be seen in (c) corresponding extra diffraction spot shown by arrow 2 in (d). The diffraction pattern shown in (d) corresponds to (a), (b) and (c). An MC carbide showing crystallinity at 1.1 dpa, (e) in bright-field, (f) showing the diffraction pattern, and (g) in precipitate dark-field with the reflection indicated by an arrow in (f). (e) and (g) are from the same region. $M_{23}C_6$ carbides in bright- and dark-field contrast with increasing dose, (h) 0.5 dpa, (i) 1.1 dpa and (j) 9.6 dpa. Dark-field images were derived from the outer diffuse ring. The size of precipitates appears to be unchanged by irradiation.

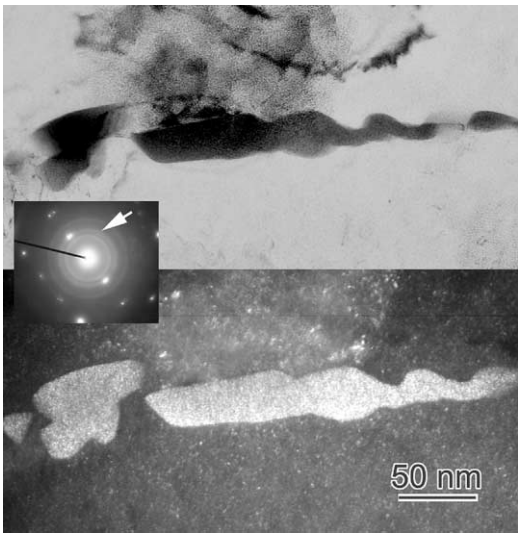

Fig. 4. Bright-field and dark-field images of $M_{23}C_6$ with diffraction pattern inset. The dark-field image was taken with the diffuse ring, which is indicated by an arrow. Very small structures appeared to be contained within in the $M_{23}C_6$ carbides at 9.6 dpa.

Fig. 3(h), (i) and (j) for 0.5, 1.1 and 9.6 dpa respectively, as shown in both bright-field and dark-field images.

TEM–EDS examination of carbides was performed on extraction replicas of irradiated and unirradiated 9Cr–1Mo. The carbides were $M_{23}C_6$ with an average composition of (78–92)%Nb, (2–15)%Fe, (2–8)%Cr, (0–4)%V, (0–2)%Mn. EDS analysis revealed no detectable difference in the composition of carbides before and after irradiation.

High-magnification, dark-field images of $M_{23}C_6$ carbides (1.1 dpa) taken with the diffuse ring (marked by an arrow seen in Fig. 4) appear to show very small microcrystallites within the $M_{23}C_6$ carbides. $M_{23}C_6$ carbides were therefore investigated by high-resolution electron microscopy to assess this possibility. Lattice imaging revealed that $M_{23}C_6$ carbides were indeed amorphous, as shown in Fig. 5.

4. Discussion

Mixed proton and spallation neutron irradiation in LANSCE produced a significant change in the microstructure of 9Cr–1Mo at these low temperatures. Black-spot damage was the most common feature at all dpa levels. Electron diffraction patterns did not reveal any radiation-induced precipitation.

Helium and hydrogen gas measurements on 9Cr–1Mo from the same experiment have been reported [6]. 9Cr–1Mo has retained ~135 appm helium and ~744 appm hydrogen at 1.1 dpa, and retained ~1750 appm helium and ~4300 appm hydrogen at 9.6 dpa ~190 appm helium and ~420 appm hydrogen was retained for per dpa in 9Cr–1Mo ferritic/martensitic steel. There was, however, no indication of any void or bubble formation, even at the highest gas levels. In the temperature range 32–57 °C, it appears that there is insufficient mobility of helium atoms to allow nucleation and growth of bubbles or voids. However, void swelling is well known to occur in ferritic/martensitic steels at higher temperatures (>400 °C) [7,8].

At such low temperatures (<60 °C), neutron and proton irradiation data for 9Cr–1Mo for comparison with our results are very limited. 9 Cr–1Mo and HT9 irradiated in HFIR at 55 °C to 10 dpa showed an increase in tensile strength and microhardness [9]. TEM examinations of these alloys at 10 dpa revealed small defect clusters (black-spot damage) and dislocations. However, these dislocations were not induced by

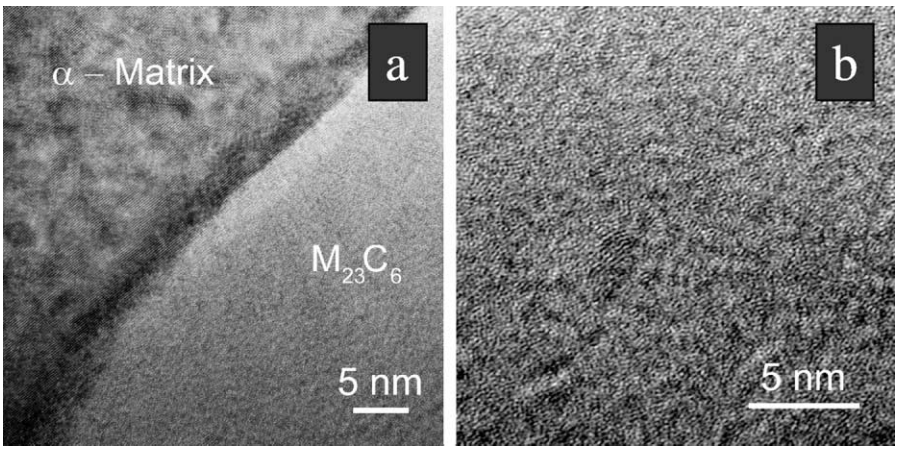

Fig. 5. Irradiated 9Cr–1Mo showing (a) the interface of α-matrix and $M_{23}C_6$ carbide, and (b) lattice image of $M_{23}C_6$ carbide at 1.1 dpa.

irradiation. Furthermore, the pre-existing distributions of $M_{23}C_6$ carbides, as well as martensite lath structure remained unchanged [10].

Investigation of DIN type martensitic steel after irradiation with 800 MeV protons [11] revealed a crystalline-to-amorphous transformation of $M_{23}C_6$ carbides, and also formation of small Frank loops at temperatures less than 250 °C. No cavity formation was observed in this study.

A recent publication [12] on F82H ferritic/martensitic steel irradiated with 590 MeV protons, protons and fission neutrons, and fission neutrons at temperatures ranging from room temperature to 310 °C, also indicated that amorphization of carbides occurred under certain conditions. Carbides were amorphous after irradiation with protons to a dose of 1.7 dpa at room temperature, but, in all other cases (>250 °C), the carbides remained crystalline.

Many crystalline materials undergo a crystalline-to-amorphous phase transition when subjected to energetic particle irradiation at low temperatures. A number of studies have been published on crystalline-to-amorphous transitions in oxides and metallic systems (ordered phases) [13–15]. When an oxide is ion-bombarded, its tendency to amorphize or crystallize can be understood in terms of either a temperature-ratio or a bond-type criterion. A physical model involving thermal spikes states that amorphization should occur whenever the ratio T_c/T_m (T_c: crystallization temperature/T_m: melting point) exceeds 0.30 [13]. The bond-type criterion states that amorphization should occur whenever the ionicity is equal to or smaller than 0.47 for oxides. For metallic systems a generalized version of the Lindemann melting criterion has been used as a conceptual basis for a unified thermodynamic description of heat-induced melting and disorder-induced amorphization [15].

In addition, examination of the influence of hydrogen on the electron-irradiation-induced amorphization of Zr_2Ni and Zr_3Al showed that hydrogen solutes can significantly increase the upper temperature at which electron-induced amorphization is possible [16]. When irradiations are performed at temperatures close to the upper temperature at which amorphization would be possible in hydrogen-free material, the presence of hydrogen significantly reduces the dose required to produce complete amorphization. Amorphization of $M_{23}C_6$ carbides from the current study, however, has only been confirmed under the combined conditions of low temperature and high gas concentration. Temperature is one of the controlling parameters. Hydrogen, having some limited mobility at such low temperatures, might also play a significant role in amorphization of $M_{23}C_6$ carbides by increasing the stability of the defective structure. Persistent crystallinity of MC carbides, on the other hand, might be due to the lower crystallization temperature and/or higher average shear modulus.

5. Conclusions

Mixed proton and spallation neutron irradiation <60 °C resulted in formation of small defect clusters. Radiation-induced precipitation did not occur. No cavity formation was observed in the samples examined between 0.5 and 9.6 dpa.

$M_{23}C_6$ carbides were amorphous after irradiation at temperatures between 32 and 57 °C. The amorphization of $M_{23}C_6$ carbides was complete by 0.5 dpa. In samples with a dose of 1.1 dpa and higher, $M_{23}C_6$ carbides remained amorphous, while MC carbides remained crystalline. No detectable changes occurred in either carbide composition or carbide size.

Acknowledgements

This work was conducted at Pacific Northwest National Laboratory and was supported by the US Department of Energy under the Accelerator Production of Tritium Program, managed by Los Alamos National Laboratory. Battelle Memorial Institute operates Pacific Northwest National Laboratory for USDOE.

References

[1] S.A. Maloy, W.F. Sommer, R.D. Brown, J.E. Roberts, J. Eddleman, E. Zimmerman, G. Willcutt, Progress report on the accelerator production of tritium materials irradiation program, in: M.S. Wechler, L.K. Mansur, C.L. Snead, W.F. Sommer (Eds.), Proceedings of the Symposium on Materials for Spallation Neutron Sources, TMS, Warrendale, PA, 1998, p. 35.

[2] M.R. James, S.A. Maloy, W.F. Sommer, P.D. Ferguson, M.M. Fowler, K. Corzine, in: 2nd International Topical Meeting on Nuclear Applications of Accelerator Technology, Gatlinburg, TN, 20–23 September, 1998, p. 605.

[3] G.J. Willcutt, S.A. Maloy, M.R. James, J. Teague, D.A. Siebe, W.F. Sommer, P.D. Ferguson, in: 2nd International Topical Meeting on Nuclear Applications of Accelerator Technology, Gatlinburg, TN, 20–23 September, 1998, p. 254.

[4] R. Schaublin, P. Spatig, M. Victoria, J. Nucl. Mater. 258–263 (1998) 1178.

[5] M. Ruhle, M. Wilkens, Cryst. Lattice Def. 6 (1975) 129.

[6] B.M. Oliver, F.A. Garner, S.A. Maloy, W.F. Sommer, P.D. Ferguson, M.R. James, Effects of radiation on materials, 20th International Symposium, ASTM STP 1405, in: S.T. Rosinski, M.L. Grossbeck, T.R. Allen, A.S. Kumar (Eds.), 20th International Symposium, ASTM STP 1405, American Society for Testing and Materials, West Conshohocken, PA, 2002, p. 612.

[7] D.S. Gelles, R.L. Meinecke, Alloy Development for Irradiation Performance Semiannual Progress Report, DOE/ER-045/11, 1984, p. 103.

[8] D.S. Gelles, J. Nucl. Mater. 108–109 (1982) 515.
[9] W.L. Hu, D.S. Gelles, Effects of radiation on materials, in: N.H. Packan, R.E. Stoller, A.S. Kumar (Eds.), 14th International Symposium, vol. II, ASTM STP 1046, American Society for Testing and Materials, West Conshohocken, PA, 1982, p. 453.
[10] D.S. Gelles, W.L. Hu, F.H. Huang, G.D. Johnson, Effects of HFIR irradiation at 55 °C on the microstructure and toughness of HT-9 and 9Cr–1Mo, Alloy development for irradiation performance, Semiannual Progress Report For Period Ending September 30, 1983, DOE/ER-0045/11, p. 115.
[11] Y. Dai, G.S. Bauer, F. Carsughi, H. Ullmaier, S.A. Maloy, W.F. Sommer, J. Nucl. Mater. 265 (1999) 203.
[12] R. Schaublin, M. Victoria, J. Nucl. Mater. 283–287 (2000) 339.
[13] R. Kelly, H.M. Naguib, in: Proceedings of the International Conference on Atomic Collision Phenomena in Solids, North-Holland, Amsterdam, 1970, p. 172.
[14] H.M. Naguib, R. Kelly, Radiat. Eff. 25 (1975) 1.
[15] N.Q. Lam, P.R. Okamoto, M. Li, J. Nucl. Mater. 251 (1997) 89.
[16] D.K. Tappin, I.M. Robertson, H.K. Birnbaum, Phys. Rev. B, Condens. Matt. 51 (21) (1995) 14854.